Research on Chemical Intermediates
https://doi.org/10.1007/s11164-018-3597-4

# $Fe_3O_4$-supported *N*-pyridin-4-amine-grafted graphene oxide as efficient and magnetically separable novel nanocatalyst for green synthesis of 4*H*-chromenes and dihydropyrano[2,3-*c*]pyrazole derivatives in water

**Davood Azarifar**[1] · **Masoud Khaleghi-Abbasabadi**[1]

Received: 9 July 2018 / Accepted: 10 September 2018
© Springer Nature B.V. 2018

## Abstract

$Fe_3O_4$-magnetized *N*-pyridin-4-amine-functionalized graphene oxide [$Fe_3O_4$@GO-*N*-(pyridin-4-amine)] was readily prepared via a three-step procedure. The synthesized nanofilms were characterized by scanning electron microscopy, powder X-ray diffraction analysis, Fourier-transform infrared spectroscopy, energy-dispersive X-ray spectroscopy, vibrating-sample magnetometry, and elemental analysis. The prepared magnetic amine-functionalized graphene oxide exhibited high catalytic activity for one-pot three-component synthesis of dihydropyrano[2,3-*c*]pyrazole and tetrahydrobenzo[*b*]pyran (4*H*-chromene) derivatives. Excellent product yield, short reaction time, use of water as green solvent, and easy workup procedure are the main advantages of the present protocol. In addition, the catalyst could be easily separated by magnetic decantation and reused for six cycles without significant loss of catalytic activity.

**Electronic supplementary material** The online version of this article (https://doi.org/10.1007/s11164-018-3597-4) contains supplementary material, which is available to authorized users.

✉ Davood Azarifar
azarifar@basu.ac.ir

[1] Department of Chemistry, Bu-Ali Sina University, Hamedan 65178, Iran

Published online: 28 September 2018

**Graphical abstract**

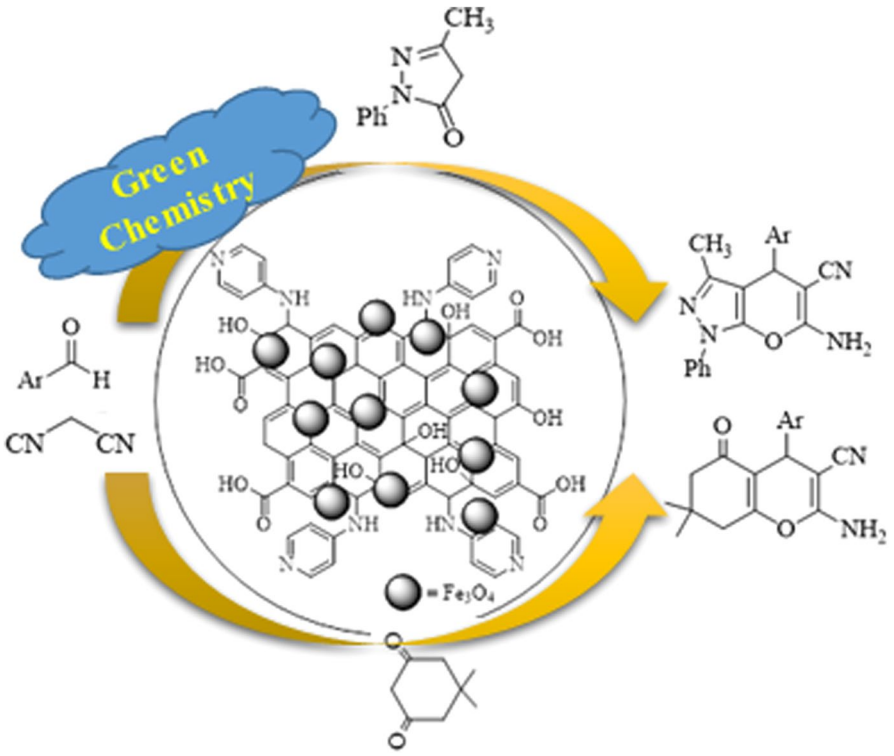


**Keywords** Magnetite-supported · *N*-pyridin-4-amine-grafted · Graphene oxide · Magnetic nanocatalyst · Dihydropyrano[2,3-*c*]pyrazoles · Tetrahydrobenzo[*b*]pyrans

## Introduction

Due to increasing concerns regarding the environment, green chemistry has emerged as an important issue, including development of green approaches and efficient recoverable heterogeneous catalysts for use in industrial processes and organic syntheses [1–3]. In recent years, heterogeneous catalysts have found wide applications as environmentally compatible materials, resulting in great interest for use in various industrial and organic transformations and syntheses [4]. Among the heterogeneous catalysts, different nanoparticles (NPs) have attracted enormous interest due to their high catalytic activity and interesting physical and chemical properties, such as high selectivity, nontoxicity, reusability, long-term stability, and high surface area to volume ratio that enables high catalyst loading capacity [5–12]. In addition, such nanosized particles are easily dispersible in solution, forming stable suspensions [13, 14]. In spite of these advantages, such small particles require tedious processes

for recycling and separation from the reaction mixture by filtration or expensive ultracentrifugation, limiting their application [15]. This problem has been tackled by using magnetic nanoparticles (MNPs) as excellent supports amenable to simple magnetic separation [16–21]. Such MNP-supported heterogeneous catalysts have found wide applications in organocatalysis and industrial catalytic processes [22, 23]. In this context, $Fe_2O_3$ and $Fe_3O_4$ nanoparticles are the most extensively studied core magnetic supports, owing to their high surface area, high catalyst loading ability, conductivity, magnetic susceptibility, catalytic activity, and striking stability [24–26].

Among the well-documented nanomaterials, nanostructured carbon materials have attracted enormous interest as environmentally compatible and efficient catalysts for use in different chemical and industrial processes, due to their interesting properties such as high corrosion resistance, air stability, and low cost [27–32]. Carbon-based nanomaterials exist in different allotropic forms such as fullerene, carbon nanotubes (CNTs), graphene, diamond, and porous carbon on zero-, one-, two-, and three-dimensional nanoscales. Graphene is a well-represented allotrope of carbon, characterized structurally by one-atom-thick planar sheets of $sp^2$-bonded carbon atoms densely packed in a two-dimensional hexagonal honeycomb crystal lattice. Graphitic materials have emerged as the most widely used carbon materials in various fields due to their outstanding properties such as appropriate electrical conductivity, high mechanical strength, suitable transparency, high surface area, and proper biocompatibility [33–38]. Graphene oxide (GO) has been reported to possess oxidative catalytic activity and has found versatile applications as an environmentally friendly and air-stable heterogeneous metal-free catalyst for use in various chemical reactions [39–41]. The structural model suggested for graphene oxide (GO) on the basis of its solid-state $^{13}C$ nuclear magnetic resonance (NMR) spectrum is shown in Fig. 1 [42]. Accordingly, GO is built of layers of six-membered aromatic rings of variable sizes, carrying different functional groups such as carboxyl, hydroxyl, and epoxy groups. Such functional groups enable the carbon layers of GO to mediate ionic and nonionic interactions with a wide range of molecules and also exhibit oxidizing and acidic effects in different reactions [40].

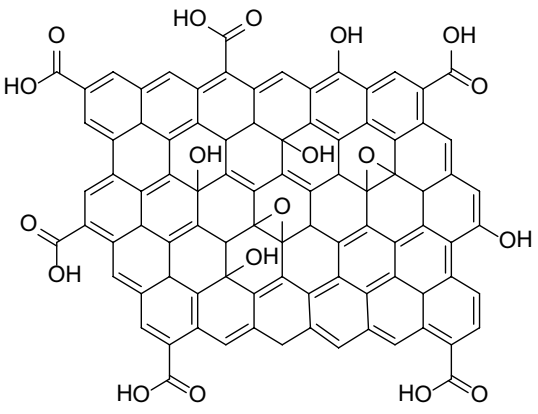


**Fig. 1** Structural model of graphene oxide (GO)

Polyfunctionalized 4*H*-chromenes have been found to exhibit intriguing biological and pharmaceutical properties such as antimicrobial [43], antileishmanial [44], antitumor [45], hypotensive [46], anti-human immunodeficiency virus (HIV) [47, 48], and local anesthetic [49] activities. 4*H*-Chromenes carrying amino and nitrile functionalities are also favored medicinal compounds showing potential anticancer activity [50, 51]. Moreover, a variety of functionalized 4*H*-chromene moieties appear as the key building block of numerous oxygen-containing natural products that exhibit diverse biological and pharmacological activities such as antitumor [52], antiallergenic [53], antiinflammatory [54], and antineurodegenerative effects [55]. In addition, chromenes have found applications in other fields such as cosmetics, pigments, and potentially biodegradable agrochemicals [56].

Conventional methods reported for synthesis of chromenes generally employ three-component condensation reaction between aldehydes, malononitrile, and 1,3-diketones. These reactions utilize different catalytic systems including hexadecyltrimethyl ammonium bromide [57], ionic liquids [58], Mg/La mixed metal oxides [59], nanosilica [60], and silica-bonded propylpiperazine-*N*-sulfamic acid [61], including reactions performed under various conditions such as electrochemical condition [60] and microwave radiation [62]. In addition, a novel magnetically immobilized organocatalyst fabricated by covalently anchoring 2-aminomethylphenol moiety on the surface of hydroxyapatite-encapsulated maghemite nanoparticles has been explored for preparation of benzo[*b*]pyrans and dihydropyrano[*c*]chromenes [63].

4*H*-Pyran-containing molecules form another important class of heterocyclic compounds that show diverse biological activities. Pyrano[2,3-*c*]pyrazoles have attracted considerable interest owing to their significant pharmacological and therapeutic values as antibacterial, anticoagulant, anticancer, diuretic, and insecticidal agents [64, 65]. These derivatives also constitute a structural unit for synthesis of some pharmaceutical agents, promising drugs, and photoactive materials [66–69].

Generally, synthesis of dihydropyrano[2,3-*c*]pyrazole derivatives involves three-component condensation reaction between 3-methyl-1-phenylpyrazolin-5-one, malononitrile, and aldehydes under catalysis by various catalytic systems such as ionic liquids [70], piperidine [71], cupreine [72], MgO [73], and hexadecyldimethylbenzyl ammonium bromide (HDMBAB) [74]. We recently described a facile, high-yielding, one-pot synthesis of pyrano[2,3-*c*]pyrazole derivatives using γ-$Fe_2O_3$@$Cu_3$Al-LDH as efficient and reusable magnetic nanocatalyst [75].

As part of our ongoing efforts towards development of newer and benign heterogeneous nanocatalysts, and their applications in catalytic organic reactions and synthesis of heterocyclic compounds [75–80], we describe herein the synthesis and characterization of $Fe_3O_4$-supported *N*-pyridin-4-amine-functionalized graphene oxide and its application as efficient and recyclable heterogeneous magnetic nanocatalyst for one-pot three-component synthesis of 4*H*-chromenes (**4a**–**h**) and dihydropyrano[2,3-*c*]pyrazoles (**5a**–**h**) (Scheme 1).

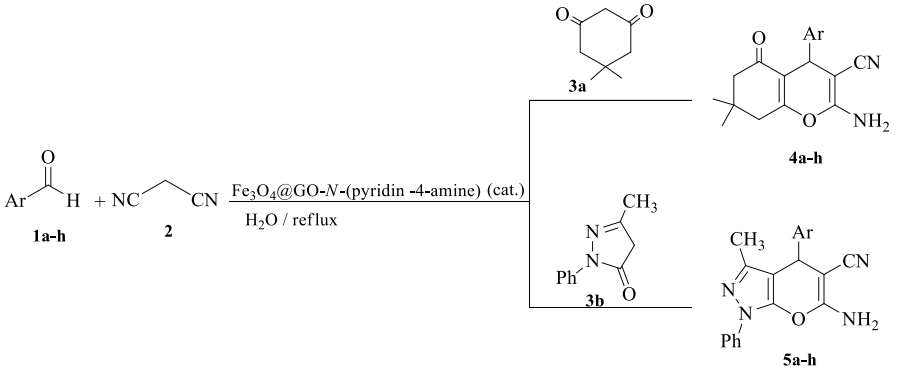


**Scheme 1** Synthesis of 4*H*-chromenes **4a**–**h** and pyrano[2,3-*c*]pyrazoles **5a**–**h** under catalysis by $Fe_3O_4$@GO-*N*-(pyridin-4-amine) nanofilms

## Experimental

### General

Chemicals including natural flake graphite (−325 mesh, 99.95 %) were purchased from Merck chemical company and used as received. Reaction progress was monitored by thin-layer chromatography (TLC) on Silica Gel PolyGram SIL G/UV 254 plates. Melting points were measured in open capillary tubes using an Electrothermal 9100 apparatus. Fourier-transform infrared (FT-IR) spectra were recorded from KBr pellets using a PerkinElmer Spectrum 65 FT-IR spectrophotometer. NMR spectra were recorded for samples in $CDCl_3$ or dimethyl sulfoxide (DMSO)-$d_6$ on 90, 300, and 400 MHz Bruker spectrometers using $Me_4Si$ as internal standard. The magnetic properties of the catalyst sample were measured with a vibrating-sample magnetometer (VSM, model LBKFB, Meghnatis Daghigh Kavir Co., Iran) at room temperature. Energy-dispersive X-ray (EDX) analysis of the prepared catalyst was performed on a VG ESCALAB-200R spectrometer equipped with a hemispherical electron analyzer. Powder X-ray diffraction (XRD) analysis was conducted on a PANalytical X'PertPRO X-ray diffractometer. Ultrasonication was performed in a 2200 ETH-SONICA ultrasound cleaner at frequency of 45 kHz. Scanning electron microscopy (SEM) images were obtained using a Tescan model MIRA 3 field emission gun-scanning electron microscope (FEG-SEM).

### Preparation of graphene oxide (GO)

Graphene oxide was prepared following the modified Hummers method [81, 82]. Initially, 250 mL $H_2SO_4$ was added to 5 g graphite powder, and the mixture was stirred for 24 h. Next, to the resulting mixture was slowly added 30 g $KMnO_4$, and the reaction mixture was continuously stirred at 50 °C for 72 h. The resulting mixture was then poured into a beaker containing 500 mL ice, followed by addition of 50 mL $H_2O_2$ (30 %) in 500 mL deionized (DI) water. As a result, the mixture turned

from brown color to bright yellow. The reaction product was separated by centrifugation, washed with DI water and 10 % HCl solution repeatedly, and dried at 60 °C.

## Preparation of $Fe_3O_4$-supported *N*-pyridin-4-amine-grafted graphene oxide magnetic nanofilms

### Functionalization of graphene oxide with *N*-pyridin-4-amine

Functionalization of graphene oxide (GO) with 4-aminopyridine takes place via nucleophilic ring-opening of epoxide groups [83]. To a dispersion of 1 g GO in 50 mL ethanol in a three-necked round-bottomed flask was added 3 g 4-aminopyridine, and the mixture was stirred for 24 h under reflux condition. Then, the reaction mixture was allowed to reach room temperature, followed by filtration to separate the product GO-*N*-(pyridin-4-amine). Finally, the solid product was repeatedly washed with deionized (DI) water and ethanol three times, and dried in an oven at 70 °C.

### Nanomagnetization of *N*-pyridin-4-amine-functionalized graphene oxide (NMAP-GO)

$Fe_3O_4$-supported *N*-pyridin-4-amine-functionalized graphene oxide [$Fe_3O_4$@GO-*N*-(pyridin-4-amine)] was prepared by coprecipitation of $FeCl_2{\cdot}4H_2O$ and $FeCl_3{\cdot}6H_2O$ in presence of 4-aminopyridine-grafted graphene oxide. Aqueous solution of $FeCl_2{\cdot}4H_2O$ and $FeCl_3{\cdot}6H_2O$ was prepared with molar ratio of 1:2. Nanomagnetization of *N*-pyridin-4-amine-functionalized graphene oxide was performed following a modified procedure reported by Kassaee et al. [84]. First, 20 mg of previously prepared *N*-pyridin-4-amine-functionalized graphene oxide [GO-*N*-(pyridin-4-amine)] in 20 mL DI water was ultrasonicated for 30 min. Then, to the resulting mixture was added 25 mL solution of $FeCl_3$ (400 mg) and $FeCl_2$ (150 mg) in DI water (20 mL) at room temperature. The feeding weight ratio of $FeCl_3$ to GO ($m_{FeCl3}$:$m_{GO}$) in the prepared mixture was 20: 1. Afterwards, the pH value of the mixture was increased to 11 by adding 30 % aqueous solution of ammonia (15 mL), and the mixture was stirred at 75 °C for 30 min. After the resulting mixture was allowed to reach room temperature, the precipitated black nanocomposite was centrifuged and washed six times with DI water, then finally dried at 70 °C to obtain pure $Fe_3O_4$@GO-*N*-(pyridin-4-amine) nanofilms.

### General procedure for synthesis of 4*H*-chromene derivatives

To a mixture of malononitrile (66 mg, 1 mmol), aromatic aldehyde **1** (1 mmol), and dimedone (14 mg, 1 mmol) in DI water (5 mL) was added $Fe_3O_4$@GO-*N*-(pyridin-4-amine) (10 mg), and the resulting mixture was stirred at reflux condition for an appropriate time (Table 3). After reaction completion as monitored by TLC, 15 mL hot EtOH was added to the resulting reaction mixture, and the catalyst was magnetically separated by using an external magnet. The solvent was removed under

reduced pressure to leave crude residue, which was recrystallized from absolute EtOH to afford pure product. The synthesized products **4a**–**h** are all known compounds and were characterized based on their melting point and spectral (FT-IR, $^1$H NMR, $^{13}$C NMR) data, in comparison with corresponding reported data (Table 3).

### General procedure for synthesis of 1,4-dihydropyrano[2,3-*c*]pyrazole derivatives

To a mixture of aldehyde **1** (1 mmol), malononitrile (66 mg, 1 mmol), and 3-methyl-1-phenyl-1*H*-pyrazol-5(4*H*)-one (174 mg, 1 mmol) in DI water (5 mL) was added the catalyst $Fe_3O_4$@GO-*N*-(pyridin-4-amine) (10 mg), and the mixture was stirred under reflux for an appropriate time (Table 5). Reaction progress was monitored by TLC. After reaction completion, the reaction mixture was diluted with hot ethanol (15 mL), and stirred for 5 min. Then, the catalyst was isolated by using an external magnet. The remaining supernatant liquid was evaporated to leave crude product, which was purified by recrystallization from absolute EtOH. All the synthesized products **5a**–**h** are known compounds and were characterized by their physical properties and spectral (FT-IR, 1H NMR, 13C NMR) analysis, in comparison with corresponding reported data (Table 5).

## Selected data

***2-Amino-7,7-dimethyl-5-oxo-4-phenyl-5,6,7,8-tetrahydro-4H-chromene-3-carbonitrile* (4a)** White solid; m.p. 235–237 °C; IR (KBr, $\nu$, $cm^{-1}$): 3394, 3324, 3251, 3212, 2960, 2889, 1680, 1604, 1413, 1371, 1249, 1214, 1159, 1138, 1071, 1036, 838, 695, 578. $^1$H NMR (90 MHz, $CDCl_3$) $\delta$: 1.04 (*s*, 3H, $CH_3$), 1.11 (*s*, 3H, $CH_3$), 2.23 (*s*, 2H, $CH_2$), 2.45 (*s*, 2H, $CH_2$), 4.41 (*s*, 1H, CH), 4.45 (*s*, 2H, $NH_2$), 7.24 (*s*, 5H, H–Ar) ppm; $^{13}$C NMR (75.5 MHz, DMSO-$d_6$) $\delta$: 26.8, 28.4, 31.8, 35.5, 49.9, 58.3, 112.7, 119.7, 127.1, 128.3, 144.7, 158.4, 162.5, 195.6 ppm.

***2-Amino-7,7-dimethyl-4-(p-fluorophenyl)-5-oxo-5,6,7,8-tetrahydro-4H-chromene-3-carbonitrile* (4b)** White solid; m.p. 188–190 °C; IR (KBr, $\nu$, $cm^{-1}$): 3354, 3178, 3100, 2960, 2190, 1674, 1636, 1603, 1504, 1410, 1366, 1261, 1215, 1160, 1139, 1033, 1015, 859, 561, 530, 487. $^1$H NMR (300 MHz, DMSO-$d_6$) $\delta$: 0.93 (*s*, 3H, $CH_3$), 1.02 (*s*, 3H, $CH_3$), 2.05–2.27 (*m*, 2H, $CH_2$), 2.50 (*s*, 2H, $CH_2$), 4.15 (*s*, 1H, CH), 6.98–7.27 (*m*, 6H, H–Ar and $NH_2$) ppm; $^{13}$C NMR (100 MHz, DMSO-$d_6$) $\delta$: 27.2, 28.8, 32.2, 35.9, 38.9, 50.4, 58.8, 113.1, 120.2, 127.1, 127.6, 128.8, 145.1, 158.9, 163.1, 196.4 ppm.

***2-Amino-4-(p-chlorophenyl)-7,7-dimethyl-5-oxo-5,6,7,8-tetrahydro-4H-chromene-3-carbonitrile* (4d)** White solid; m.p. 211–214 °C; IR (KBr, $\nu$, $cm^{-1}$): 3379, 3323, 3180, 2958, 2942, 2887, 2188, 1675, 1634, 1390, 1286, 1215, 1093, 1014, 884, 854, 769, 639, 620, 576. $^1$H NMR (90 MHz, DMSO-$d_6$) $\delta$: 0.94 (*s*, 3H, $CH_3$), 1.03 (*s*, 3H, $CH_3$), 2.15 (*s*, 2H, $CH_2$), 2.50 (*s*, 2H, $CH_2$), 4.195 (*s*, 1H, CH), 7.05–7.30 (*s*, 6H, H–Ar and $NH_2$) ppm; $^{13}$C NMR (100 MHz, DMSO-$d_6$) $\delta$:14.0, 20.7, 26.8, 28.3,

31.8, 35.1, 49.9, 57.7, 59.7, 112.3, 119.5, 128.2, 129.1, 131.1, 143.7, 158.5, 162.6, 170.3 ppm.

***2-Amino-4-(p-nitrophenyl)-7,7-dimethyl-5-oxo-5,6,7,8-tetrahydro-4H-chromene-3-carbonitrile* (4g)** Cream solid; m.p. 178–181 °C; IR (KBr, $\nu$, $cm^{-1}$): 3406, 3316, 3176, 2977, 2942, 2183, 1672, 1631, 1521, 1493, 1390, 1296, 1159, 1031, 855, 729, 629, 617, 574, 561. $^1$H NMR (90 MHz, DMSO-$d_6$) $\delta$: 0.96 (*s*, 3H, $CH_3$), 1.04 (*s*, 3H, $CH_3$), 2.17 (*s*, 2H, $CH_2$), 2.53 (*s*, 2H, $CH_2$), 4.37 (*s*, 1H, CH), 7.18–7.18 (*m*, 4H, H–Ar), 8.12 (*s*, 2H, $NH_2$) ppm. $^{13}$C NMR (100 MHz, DMSO-$d_6$) $\delta$: 26.9, 28.2, 31.8, 35.6, 39.6, 49.8, 56.9, 111.7, 119.3, 123.7, 128.6, 146.2, 152.3, 158.5, 163.1, 195.7 ppm.

***6-Amino-3-methyl-1,4-diphenyl-1,4-dihydropyrano[2,3-c]pyrazole-5-carbonitrile* (5a)** White solid; m.p. 170–173 °C; IR (KBr, $\nu$, $cm^{-1}$): 3471, 3324, 3194, 3063, 2917, 2198, 1659, 1593, 1516, 1385, 1265, 1066, 827, 753, 686, 651. $^1$H NMR (90 MHz, $CDCl_3$) $\delta$: 1.89 (*s*, 3H, $CH_3$), 4.66–4.69 (*d*, 3H, CH, $NH_2$), 7.28–7.61 (*m*, 10H, H–Ar) ppm. $^{13}$C NMR (100 MHz, DMSO-$d_6$) $\delta$: 13.0, 37.2, 58.7, 99.1, 116.5, 120.4, 126.6, 127.5, 128.2, 129.0, 129.8, 138.0, 144.0, 144.3, 145.7, 159.8 ppm.

***6-Amino-3-methyl-4-(p-chlorophenyl)-1-phenyl-1,4-dihydropyrano[2,3-c]pyrazole-5-carbonitrile* (5c)** White solid; m.p. 183–186 °C; IR (KBr, $\nu$, $cm^{-1}$): 3393, 3280, 3170, 2924, 2224, 2192, 1660, 1605, 1513, 1456, 1370, 1278, 1128, 1073, 936, 834, 759, 692, 669, 572. $^1$H NMR (400 MHz, DMSO-$d_6$) $\delta$: 1.80 (*s*, 3H, $CH_3$), 4.74 (*s*, 1H, CH), 7.28–7.81 (*m*, 11H, H–Ar and $NH_2$) ppm. $^{13}$C NMR (100 MHz, DMSO-$d_6$) $\delta$: 13.0, 36.5, 58.2, 98.7, 120.3, 120.4, 120.5, 126.7, 129.0, 129.6, 130.2, 132.1, 138.0, 143.1, 144.4, 145.7, 159.9 ppm.

***6-Amino-4-(p-methoxyphenyl)-3-methyl-1-phenyl-1,4-dihydropyrano[2,3-c]pyrazole-5-carbonitrile* (5e)** White solid; m.p. 170–173 °C; IR (KBr, $\nu$, $cm^{-1}$): 3390, 3321, 3204,3022, 2191, 1660, 1583, 1513, 1391, 1259, 11,249, 1128, 1109, 1026, 839, 759, 692, 573. $^1$H NMR (90 MHz, DMSO-$d_6$) $\delta$: 1.78 (*s*, 3H, $CH_3$), 3.74 (*s*, 3H, $CH_3$), 4.62 (*s*, 1H, CH), 6.84–7.82 (*m*, 11H, H–Ar, $NH_2$) ppm. $^{13}$C NMR (100 MHz, DMSO-$d_6$) $\delta$: 12.4, 36.1, 54.6, 59.1, 98.3, 113.4, 119.8, 125.5, 128.4, 128.7, 135.0, 137.4, 143.6, 145.2, 158.0, 158.9 ppm.

***6-Amino-4-(m-bromophenyl)-3-methyl-1-phenyl-1,4-dihydropyrano[2,3-c]pyrazole-5-carbonitrile* (5h)** White solid; m.p. 161–164 °C; IR (KBr, $\nu$, $cm^{-1}$): 3450, 3324, 3195, 2199, 1660, 1593, 1518, 1487, 1456, 1391, 1126, 1065, 859, 751, 686. $^1$H NMR (400 MHz, DMSO-$d_6$) $\delta$: 1.81 (*s*, 3H, $CH_3$), 4.75 (*s*, 1H, CH), 7.29–7.35 (*m*, 5H, H–Ar), 7.47–7.52 (*m*, 4H, H–Ar), 7.79–7.81 (*m*, 2H, $NH_2$) ppm. $^{13}$C NMR (100 MHz, DMSO-$d_6$) $\delta$: 13.1, 36.8, 58.0, 98.5, 120.4, 120.6, 122.3, 126.7, 127.5, 129.8, 130.5, 130.9, 131.3, 138.0, 144.4, 145.6, 146.9, 160.0 ppm.

## Results and discussion

### Characterization of the catalyst $Fe_3O_4$@GO-*N*-(pyridin-4-amine)

As shown in Scheme 2, $Fe_3O_4$-supported 4-aminopyridine-functionalized graphene oxide [$Fe_3O_4$@GO-*N*-(pyridin-4-amine)] was prepared using the modified method reported by Kassaee et al. [84]. As described above, graphene oxide (GO) was initially prepared via oxidation of graphite powder with $KMnO_4$ and $H_2O_2$ (30 %) in acidic solution according to the Hummers method [81]. Then, the graphene oxide (GO) was aminated through nucleophilic ring-opening of the epoxy groups in graphene oxide (GO) thin films upon treatment with 4-aminopyridine [83]. Finally,

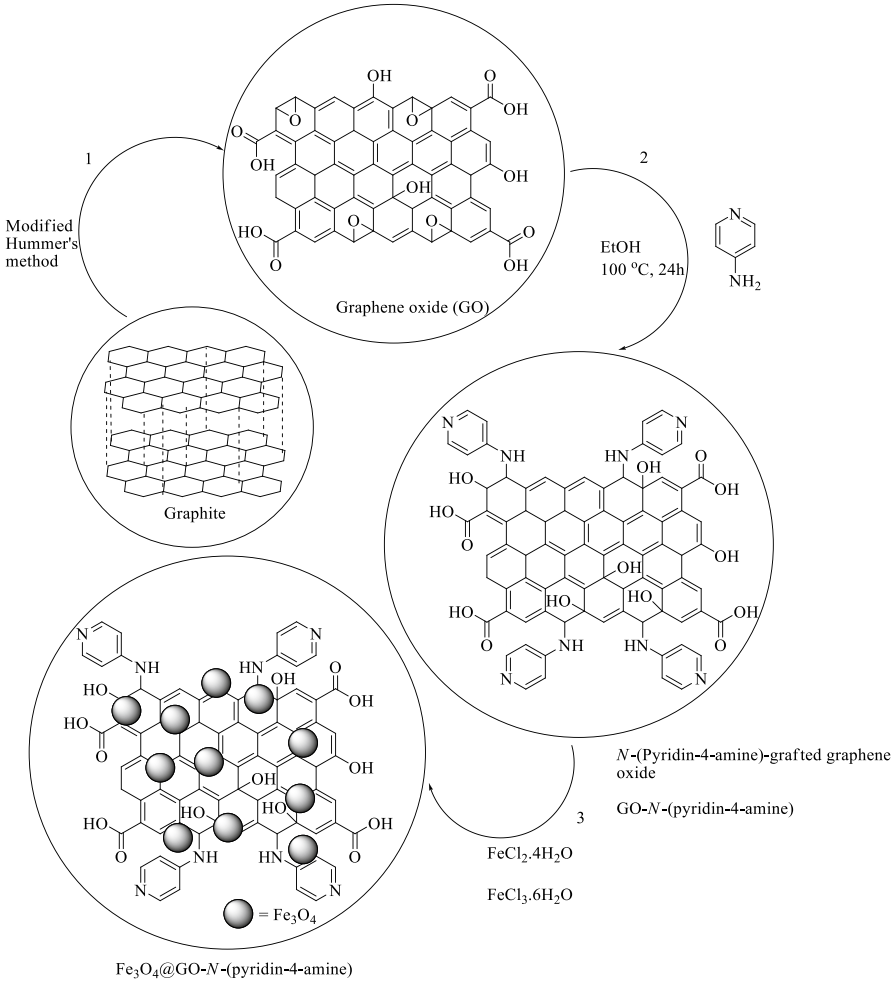


**Scheme 2** Synthetic route to nanomagnetic $Fe_3O_4$-supported 4-aminopyridine-grafted GO [$Fe_3O_4$@GO-*N*-(pyridin-4-amine)]

novel $Fe_3O_4$ magnetic $Fe_3O_4$@GO-*N*-(pyridin-4-amine) nanosheets were obtained by coprecipitation of ferrous ($Fe^{2+}$) and ferric ($Fe^{3+}$) ions in the presence of the resulting aminated graphene oxide.

The structure of the synthesized nanofilms was fully characterized by different analytical techniques including Fourier-transform infrared (FT-IR) spectroscopy, energy-dispersive X-ray (EDX) spectroscopy, scanning electron microscopy (SEM), X-ray diffraction (XRD) analysis, and vibrating-sample magnetometry (VSM).

Figure 2 illustrates the Fourier-transform (FT)-IR spectra of unfunctionalized graphene oxide (GO), *N*-(pyridine-4-amine)-functionalized GO, and $Fe_3O_4$-magnetized GO-*N*-(pyridin-4-amine) nanofilms. The O–H stretching vibration assigned to enolic, carboxylic, and hydroxy groups of GO is observed in the range of 2700–3500 $cm^{-1}$ for all three compounds. The peaks at 1717, 1620, and 1056 $cm^{-1}$ in the spectrum of graphene oxide are assigned to stretching vibrations of C=O, C=C, and C–O groups, respectively, being shifted to lower frequencies in Fig. 2b, c. In addition, the characteristic peak at 1385 $cm^{-1}$ in the spectra of pure GO can be attributed to asymmetric stretching vibration of C–O–C moiety in epoxide groups, disappearing in Fig. 2b, c. This result clearly confirms successful functionalization of the GO films with aminopyridine group. Stretching vibrations of Fe–O bond were observed at 588 and 627 $cm^{-1}$ in the spectrum of $Fe_3O_4$@GO-*N*-(pyridin-4-amine) nanofilms (Fig. 2c). The peak at 1221 $cm^{-1}$ in Fig. 2b and the peak at 1230 $cm^{-1}$ in Fig. 2c are attributed to stretching vibration of amino C–N bond formed by amination of the GO films with 4-aminopyridine. Moreover, the characteristic stretching vibrations appearing at 3300 and 3359 $cm^{-1}$ in the spectra of 4-aminopyridine-functionalized GO (Fig. 2b) and $Fe_3O_4$-magnetized GO (Fig. 2c) correspond respectively to N–H bond overlapped by O–H stretching vibration. Presence of pyridine ring is also confirmed by the appearance of the C–H stretching frequency near 3158 $cm^{-1}$, as well as the C=C and C=N stretching frequencies at 1569 and 1622 $cm^{-1}$ and near 1400 $cm^{-1}$ [85]. It is seen that the stretching frequency of carboxylic group at 1717 $cm^{-1}$ for graphene oxide was shifted to lower frequency of 1622 $cm^{-1}$ for

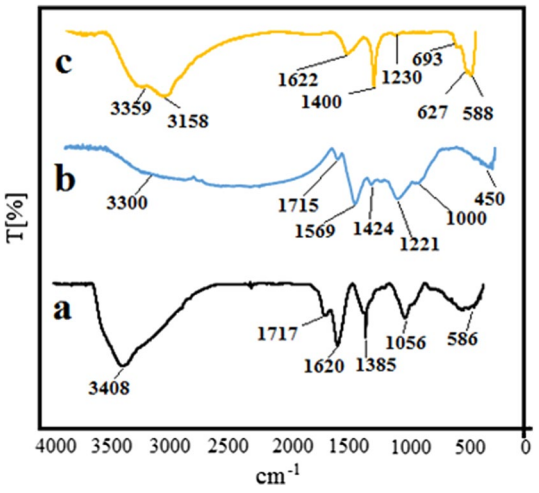


**Fig. 2** Comparative FT-IR spectra for **a** GO, **b** 4-aminopyridine-functionalized GO, and **c** $Fe_3O_4$@GO-*N*-(pyridin-4-amine) nanofilms

$Fe_3O_4$-magnetized GO. These results demonstrate that graphene oxide was successfully grafted with 4-aminopyridine groups, as further supported by magnetic $Fe_3O_4$ group.

The XRD patterns of GO and the prepared $Fe_3O_4$@GO-*N*-(pyridin-4-amine) magnetic nanofilms are presented in Fig. 3. The XRD pattern of GO shows two main diffraction peaks at $2\theta = 11.95°$ and 42.45°, corresponding to oxygen functional groups which are intercalated between the graphene sheets in the course of oxidation [87]. These peaks are related to their corresponding indices (002) and (100), respectively, and are included in the XRD pattern of the $Fe_3O_4$@GO-*N*-(pyridin-4-amine) nanofilms. As evident from the XRD pattern of $Fe_3O_4$@GO-*N*-(pyridin-4-amine) (Fig. 3b), the intensity of the peak at $2\theta = 11.8°$ exhibited by GO was significantly decreased upon amination and magnetization with $Fe_3O_4$. However, the observation of this peak at about $2\theta = 10.08°$ agrees well with the presence of oxygen functionalities, even after functionalization and magnetization of graphene oxide. The relative intensities and positions of all the peaks seen at $2\theta = 30.39°$, 35.74°, 43.36°, 57.31°, and 62.93° in the XRD pattern of $Fe_3O_4$@GO-*N*-(pyridin-4-amine) are in

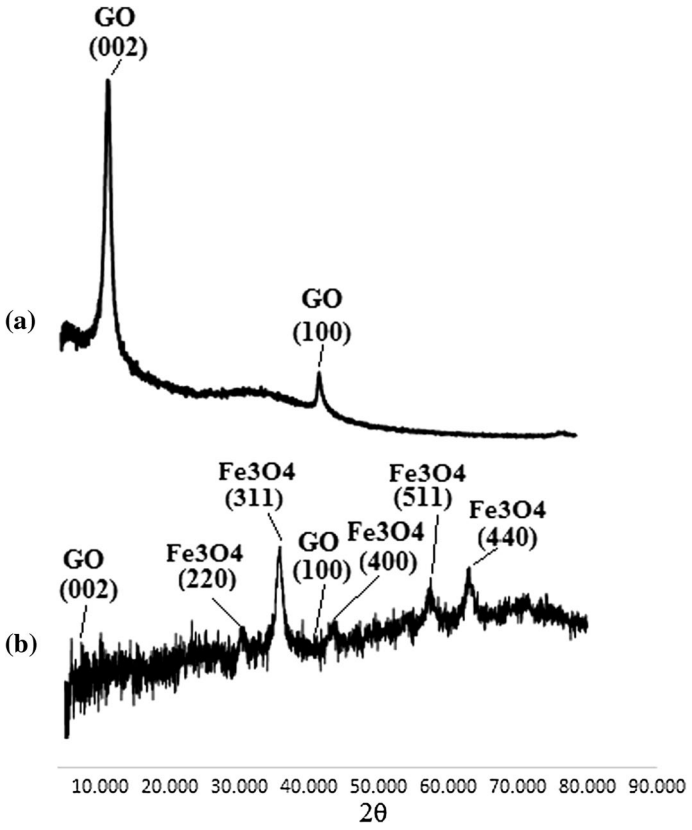


**Fig. 3** XRD patterns of **a** GO and **b** $Fe_3O_4$@GO-*N*-(pyridin-4-amine)

compliance with the standard XRD pattern of magnetite $Fe_3O_4$ in Joint Committee on Powder Diffraction Standards (JCPDS) card no. 79-0417. These five characteristic peaks, revealing a crystalline cubic structure of iron oxide phase, are related to their corresponding faces (220), (311), (400), (511), and (440), respectively. The average crystalline size of $Fe_3O_4$@GO-*N*-(pyridin-4-amine) was calculated to be 10.7 nm by Scherrer's equation for the (311) reflection with the highest intensity. This implies that GO films were successfully grafted with 4-aminopyridine groups and magnetized with $Fe_3O_4$ [86, 88].

Figure 4 presents the energy-dispersive X-ray (EDX) spectra of GO, GO-*N*-(pyridin-4-amine), and $Fe_3O_4$@GO-*N*-(pyridin-4-amine). As illustrated by these EDX results, the expected elemental constituents were obtained for graphene oxide (C, O), GO-*N*-(pyridin-4-amine) (C, O, N,) and $Fe_3O_4$@GO-*N*-(pyridin-4-amine) (C, O, N, Fe). The mass percentages of the corresponding elements calculated from the EDX analysis are presented in Table 1. These results provide further evidence of successful grafting of GO films with 4-aminopyridine group as well as magnetization with $Fe_3O_4$ MNPs.

SEM analysis was performed on the prepared films of GO, GO-*N*-(pyridin-4-amine), and $Fe_3O_4$@GO-*N*-(pyridin-4-amine) to determine their morphology and size distribution. The SEM images displayed in Fig. 5 indicate that both GO-*N*-(pyridin-4-amine) and $Fe_3O_4$@GO-*N*-(pyridin-4-amine) were composed of wrinkled thin films, closely associated with each other to form disordered solids and randomly accumulated. As revealed by comparison of the SEM images of bare GO and GO-*N*-(pyridin-4-amine), no prominent change in the morphology of the graphene films occurred as a result of functionalization. Moreover, the SEM image of the $Fe_3O_4$@GO-*N*-(pyridin-4-amine) catalyst (Fig. 5c) indicates that the $Fe_3O_4$ nanoparticles

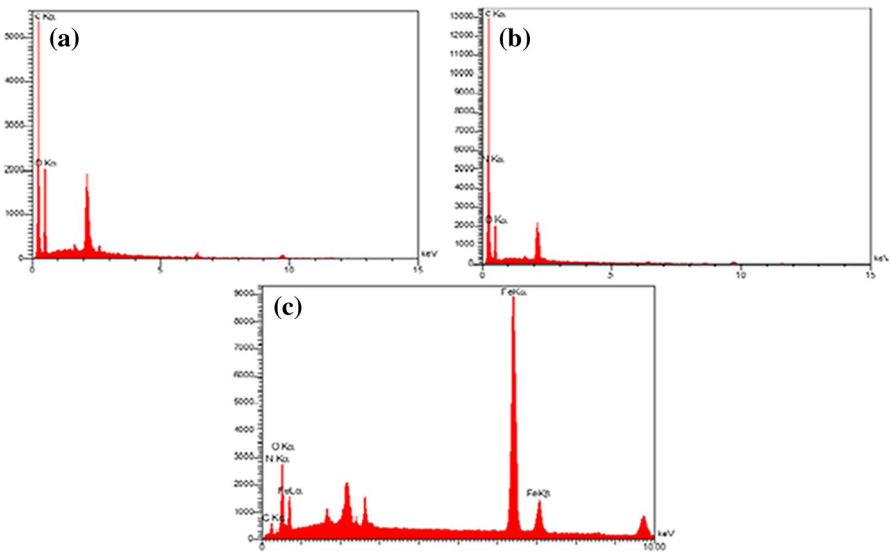


**Fig. 4** EDX results for **a** GO, **b** GO-*N*-(pyridin-4-amine), and **c** $Fe_3O_4$@GO-*N*-(pyridin-4-amine)

**Table 1** Quantitative elemental analysis of GO, GO-*N*-(pyridin-4-amine), and $Fe_3O_4$@GO-*N*-(pyridin-4-amine) derived from EDX

| Element | GO-*N*-(pyridin-4-amine) | | $Fe_3O_4$@GO-*N*-(pyridin-4-amine) | | GO | |
|---|---|---|---|---|---|---|
| | wt% | at.% | wt% | at.% | wt% | at.% |
| C | 51.51 | 57.68 | 6.35 | 17.5 | 46.40 | 53.55 |
| O | 35.39 | 29.75 | 16.76 | 34.16 | 53.60 | 46.45 |
| N | 13.10 | 12.57 | 2.12 | 4.94 | – | – |
| Fe | – | – | 74.77 | 43.65 | – | – |
| Total | 100.00 | 100.00 | 100.00 | 100.00 | 100.00 | 100.00 |

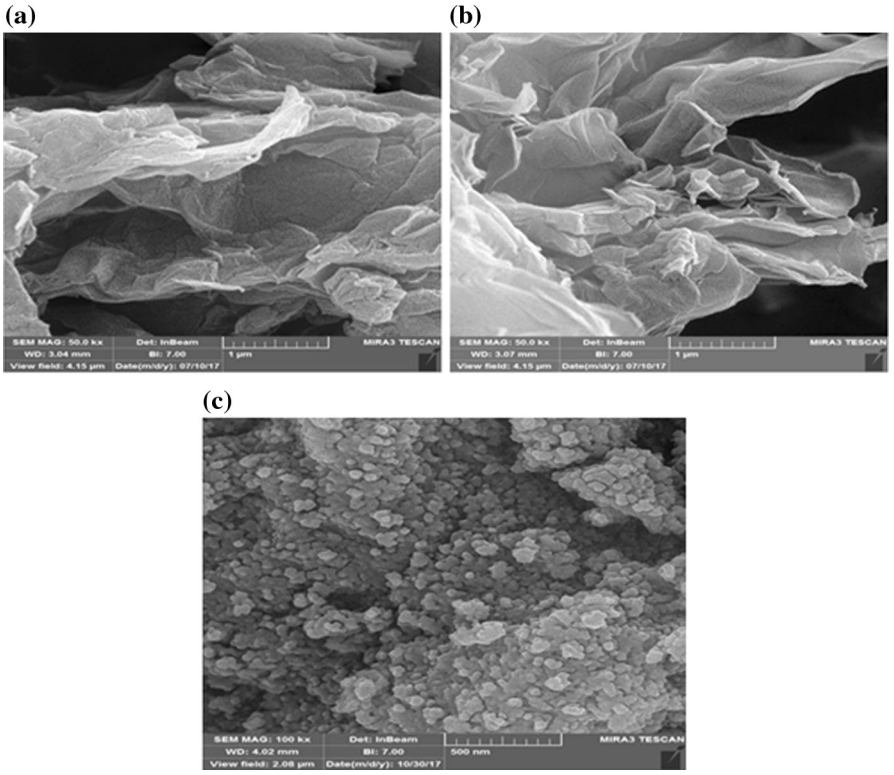


**Fig. 5** SEM images of **a** GO, **b** GO-*N*-(pyridin-4-amine), and **c** $Fe_3O_4$@GO-*N*-(pyridin-4-amine)

exhibited a regularly spherical morphology on $Fe_3O_4$@GO-*N*-(pyridin-4-amine) formed of nanosized films with average diameter of about 40 nm [84].

The magnetic behavior of the prepared $Fe_3O_4$@GO-*N*-(pyridin-4-amine) was examined by vibrating-sample magnetometry (VSM) analysis at 300 K. According to the typical plot of magnetization versus applied magnetic field of $Fe_3O_4$@GO-*N*-(pyridin-4-amine) shown in Fig. 6, the saturation magnetization ($M_s$) value of the $Fe_3O_4$@GO-*N*-(pyridin-4-amine) was found to be 48 emu $g^{-1}$. This value confirms

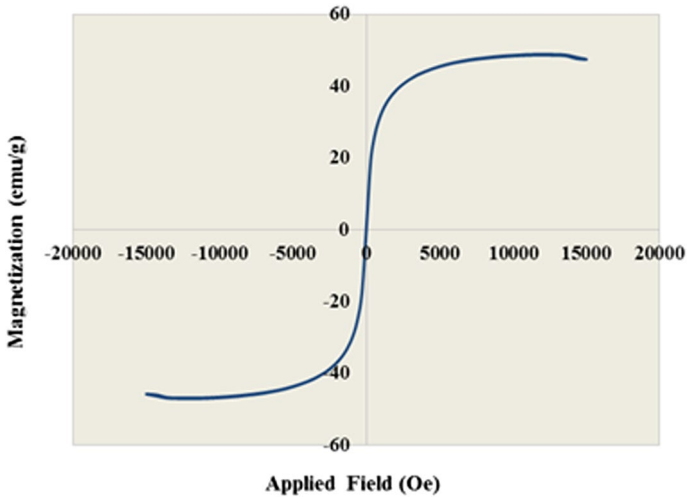


**Fig. 6** VSM results of $Fe_3O_4$@GO-*N*-(pyridin-4-amine)

the superparamagnetic property of the $Fe_3O_4$@GO-*N*-(pyridin-4-amine) nanocatalyst, which can be efficiently separated from the reaction mixture simply by using an external magnet.

## Catalytic activity

The activity of the synthesized $Fe_3O_4$@GO-*N*-(pyridin-4-amine) nanofilms as heterogeneous catalyst was tested in synthesis of 4*H*-chromenes and dihydropyrano[2,3-*c*]pyrazole derivatives. The procedure involves multicomponent one-pot cyclization reaction between aromatic aldehyde, malononitrile, and dimedone/3-methyl-1-phenyl-1*H*-pyrazol-5(4*H*)-one, as shown in Scheme 1. To investigate the feasibility of formation of the expected products and the reaction conditions, we initially employed the one-pot three-component reaction of 4-nitrobenzaldehyde, malononitrile, and 5,5-dimethyl-1,3-cyclohexanedione (dimedone) as model reaction; the results are presented in Table 2. To study the effect of solvent on this reaction, the reaction was performed using different solvents such as $H_2O$, EtOH, dimethylformamide (DMF), and tetrahydrofuran (THF) in presence of the same amount (10 mg) of catalyst at room temperature. Among the different solvents used, the best result was obtained with $H_2O$ as solvent of choice (Table 2, entry 2). It is probable that the high polarity and ability to form hydrogen bonding make water a better solvent relative to the other solvents tested in this reaction. In the next stage, the effect of temperature on the reaction was studied by conducting the reaction at higher temperatures (50, 80, 100 °C, and reflux point) in water with 10 mg catalyst. The best result in terms of reaction yield and time was obtained when the reaction was carried out in $H_2O$ under reflux condition (entry 9). Then, the catalyst loading effect was investigated in this reaction procedure; the optimal amount of catalyst was found to be 10 mg to synthesize the highest yield of product (entry 9). From the results in Table 2, it

**Table 2** Screening reaction parameters for model synthesis of 2-amino-4-(*p*-nitrophenyl)-7,7-dimethyl-5-oxo-5,6,7,8-tetrahydro-4*H*-chromene-3-carbonitrile[a]

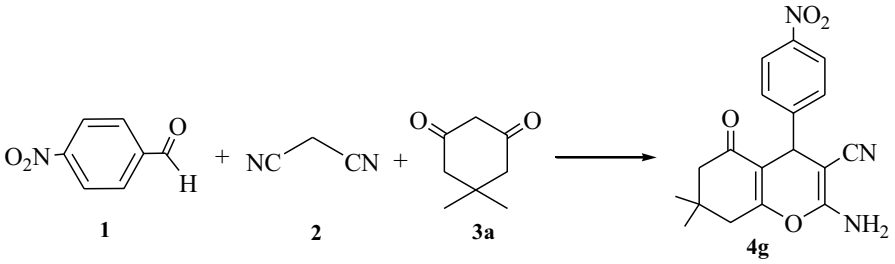


| Entry | Catalyst loading (mg) | Solvent | Temperature (°C) | Time (min) | Yield[b] (%) |
|---|---|---|---|---|---|
| 1 | 10 | No solvent | 25 | 240 | 10 |
| 2 | 10 | $H_2O$ | 25 | 60 | 65 |
| 3 | 10 | EtOH | 25 | 90 | 45 |
| 4 | 10 | THF | 25 | 180 | 25 |
| 5 | 10 | DMF | 25 | 240 | 35 |
| 6 | 10 | $H_2O$ | 50 | 50 | 72 |
| 7 | 10 | $H_2O$ | 80 | 45 | 85 |
| 8 | 10 | $H_2O$ | 100 | 40 | 87 |
| 9 | 10 | $H_2O$ | Reflux | 15 | 98 |
| 10 | 5 | $H_2O$ | Reflux | 50 | 80 |
| 11 | 20 | $H_2O$ | Reflux | 45 | 82 |
| 12 | 30 | $H_2O$ | Reflux | 45 | 84 |
| 13 | 40 | $H_2O$ | Reflux | 40 | 87 |
| 14 | No catalyst | $H_2O$ | Reflux | 240 | Trace |

[a]Conditions: 4-nitrobenzaldehyde (1.1 mmol), 4-hydroxyquinolin-2(1*H*)-one (1 mmol), malononitrile (1.1 mmol), solvent (5 mL)

[b]Isolated yield

is clear that 10 mg catalyst loading provided the best conversion. No further yield improvement was observed when increasing or reducing the amount of catalyst in the reaction (entries 9–13). To verify the indispensability of the catalyst $Fe_3O_4$@GO-*N*-(pyridin-4-amine) in the reaction, the reaction was also conducted in absence of catalyst, with no respective product being formed in detectable amount (entry 14).

The general applicability of the reaction was investigated by carrying out the reaction using a diverse series of aldehydes (**1a**–**h**) bearing various substituent groups under the optimized reaction conditions (Scheme 1). According to the experimental results summarized in Table 3, the aldehydes all reacted efficiently to afford the respective products **4a**–**h** in excellent yield (92–98 %), irrespective of the nature of the substituent groups.

**Table 3** Synthesis of 2-amino-4-aryl-7,7-dimethyl-5-oxo-5,6,7,8-tetrahydro-4*H*-chromene-3-carbonitrile derivatives catalyzed by $Fe_3O_4$@GO-*N*-(pyridin-4-amine)[a]

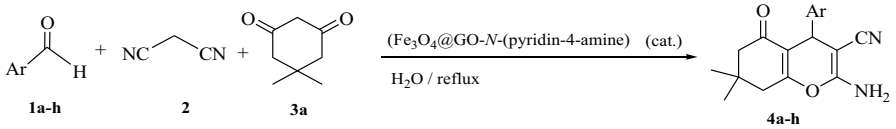


| Entry | Ar | Product | Time (min) | Yield (%) | M.p. (°C) | |
|---|---|---|---|---|---|---|
| | | | | | Found | Reported |
| 1 | $C_6H_5$ | **4a** | 30 | 94 | 235–237 | 236–238 [89] |
| 2 | 4-$FC_6H_4$ | **4b** | 20 | 96 | 188–190 | 189–191 [90] |
| 3 | 4-$MeC_6H_4$ | **4c** | 40 | 92 | 207–210 | 208–210 [77] |
| 4 | 4-$ClC_6H_4$ | **4d** | 30 | 92 | 211–214 | 212–214 [91] |
| 5 | 2-$ClC_6H_4$ | **4e** | 35 | 94 | 211–214 | 212–214 [91] |
| 6 | 3-$NO_2C_6H_4$ | **4f** | 35 | 95 | 209–212 | 210–211 [92] |
| 7 | 4-$NO_2C_6H_4$ | **4g** | 15 | 98 | 178–181 | 178–180 [92] |
| 8 | 4-$HOC_6H_4$ | **4h** | 25 | 95 | 203–206 | 204–205 [93] |

[a]Conditions: aldehyde (1.1 mmol), dimedone (1 mmol), malononitrile (1.1 mmol), $H_2O$ (5 mL), catalyst (10 mg), reflux temperature

[b]Isolated yield

The versatility and catalytic potential of the prepared catalyst were further studied in one-pot condensation reaction between aromatic aldehydes, malononitrile, and 3-methyl-1-phenyl-2-pyrazolin-5-one for synthesis of 1,4-dihydropyrano[2,3-*c*]pyrazoles **5a**–**h** (Scheme 1). Similarly, 4-nitrobenzaldehyde was chosen as test aromatic compound in this reaction to establish the reaction conditions. First, the effect of solvent on this reaction was studied using different solvents ($H_2O$, EtOH, DMF, and THF) in presence of 10 mg catalyst at room temperature. Considering the experimental results summarized in Table 4, the solvent of choice was found to be $H_2O$ in terms of reaction yield and time (entry 9). Further experiments were carried out to study the effect of higher temperatures (50, 80, 100 °C, and reflux point), revealing that the best result was achieved at reflux temperature (entry 9). Then, the effect of the catalyst loading was studied; the optimal amount of catalyst was found to be 10 mg (entry 9). Finally, the catalytic role of the catalyst was verified by performing the reaction without catalyst, resulting in no detectable amount of product after a long reaction time (entry 14).

After optimization of the reaction conditions, the scope and generality of the reaction were investigated by conducting the reaction with a diverse series of aromatic aldehydes (**1a**–**h**) holding various substituent groups under the optimized conditions (Scheme 1). The experimental results summarized in Table 5 show that all the reactions proceeded smoothly to afford the products in excellent yields, irrespective of the nature of the substituents. However, aromatic

**Table 4** Screening reaction parameters for the model synthesis of 6-amino-3-methyl-4-(*p*-nitrophenyl)-1-phenyl-1,4-dihydropyrano[2,3-*c*]pyrazole-5-carbonitrile[a]

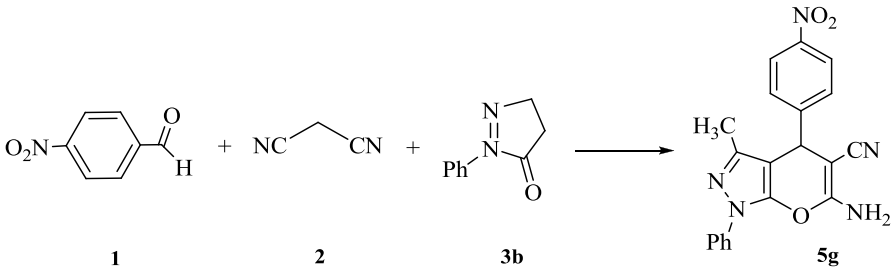


**1** **2** **3b** **5g**

| Entry | Catalyst loading (mg) | Solvent | Temperature (°C) | Time (min) | Yield[b] (%) |
|---|---|---|---|---|---|
| 1 | 10 | No solvent | 25 | 180 | Trace |
| 2 | 10 | $H_2O$ | 25 | 60 | 55 |
| 3 | 10 | EtOH | 25 | 90 | 50 |
| 4 | 10 | THF | 25 | 180 | 30 |
| 5 | 10 | DMF | 25 | 180 | 42 |
| 6 | 10 | $H_2O$ | 50 | 35 | 75 |
| 7 | 10 | $H_2O$ | 80 | 45 | 85 |
| 8 | 10 | $H_2O$ | 100 | 35 | 85 |
| 9 | 10 | $H_2O$ | Reflux | 20 | 98 |
| 10 | 5 | $H_2O$ | Reflux | 45 | 82 |
| 11 | 20 | $H_2O$ | Reflux | 50 | 70 |
| 12 | 30 | $H_2O$ | Reflux | 75 | 77 |
| 13 | 40 | $H_2O$ | Reflux | 75 | 80 |
| 14 | No catalyst | $H_2O$ | Reflux | 180 | Trace |

[a]Conditions: 4-nitrobenzaldehyde (1.1 mmol), 4-hydroxyquinolin-2(1*H*)-one (1 mmol), malononitrile (1.1 mmol), solvent (5 mL)

[b]Isolated yield

aldehydes carrying electron-withdrawing groups appeared to act more readily in this reaction.

Table 6 compares the experimental results (reaction time, yield, and conditions) obtained from the present protocol with results reported by other research groups for catalytic synthesis of 2-amino-4-aryl-7,7-dimethyl-5-oxo-5,6,7,8-tetrahydro-4*H*-chromene-3-carbonitrile (**4a**–**h**) and 1,4-dihydropyrano[2,3-*c*]pyrazole (**5a**–**h**) derivatives. Based on this comparison, our method appears more convenient in utilizing $H_2O$ as green solvent and an ecofriendly and efficient recyclable new magnetic nanocatalyst for synthesis of 2-amino-4-aryl-7,7-dimethyl-5-oxo-5,6,7,8-tetrahydro-4*H*-chromene-3-carbonitrile (entry 5) and 1,4-dihydropyrano[2,3-*c*]pyrazole (entry 10) derivatives in short reaction time and high yield. The high EcoScale score of the present protocol calculated from

**Table 5** Synthesis of 1,4-dihydropyrano[2,3-*c*]pyrazole derivatives catalyzed by $Fe_3O_4$@GO-*N*-(pyridin-4-amine)[a]

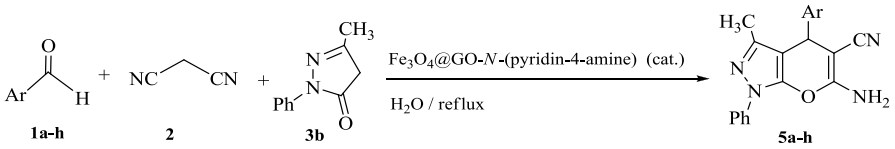


**1a-h** **2** **3b** **5a-h**

| Entry | Ar | Product | Time (min) | Yield[b] (%) | M.p. (°C) | |
|---|---|---|---|---|---|---|
| | | | | | Found | Reported |
| 1 | $C_6H_5$ | **5a** | 30 | 94 | 170–173 | 170–171 [94] |
| 2 | 2-$ClC_6H_4$ | **5b** | 30 | 96 | 145–148 | 145–146 [95] |
| 3 | 4-$ClC_6H_4$ | **5c** | 35 | 97 | 183–186 | 184–187 [96] |
| 4 | 4-$FC_6H_4$ | **5d** | 25 | 96 | 173–176 | 174–177 [96] |
| 5 | 4-$MeOC_6H_4$ | **5e** | 40 | 93 | 170–173 | 171–172 [96] |
| 6 | 3-$NO_2C_6H_4$ | **5f** | 35 | 92 | 190–193 | 190–191 [95] |
| 7 | 4-$NO_2C_6H_4$ | **5g** | 20 | 98 | 186–189 | 186–188 [97] |
| 8 | 3- $BrC_6H_4$ | **5h** | 30 | 94 | 161–164 | 160–163 [98] |

[a]Conditions: aldehyde (1.1 mmol), 3-methyl-1-phenyl-2-pyrazolin-5-one (1 mmol), malononitrile (1.1 mmol), $H_2O$ (5 mL), catalyst (10 mg), reflux temperature

[b]Isolated yield

**Table 6** Comparison of catalytic efficiency of present protocol with reported catalysts for synthesis of 2-amino-4-aryl-7,7-dimethyl-5-oxo-5,6,7,8-tetrahydro-4*H*-chromene-3-carbonitrile and 1,4-dihydropyrano[2,3-*c*]pyrazole based on EcoScale percentages and other reaction parameters

| Product | Catalyst | Conditions | Time (min) | Yield (%) | EcoScale (%) | Ref. |
|---|---|---|---|---|---|---|
| **4g** | Pectin | $H_2O$:EtOH; r.t. | 20 | 90 | 90 | [99] |
| **4g** | Fructose | EtOH:$H_2O$; 40 °C | 10 | 89 | 87 | [100] |
| **4g** | $NH_4Al(SO_4)_2{\cdot}12H_2O$ | EtOH; 80 °C | 140 | 85 | 84 | [101] |
| **4g** | [DABCO-PDO][$CH_3COO$] | $H_2O$; 60 °C | 10 | 96 | 90 | [102] |
| **4g** | $Fe_3O_4$@GO-*N*-(pyridin-4-amine) | $H_2O$; reflux | 15 | 98 | 91 | Present work |
| **5g** | $NH_4H_2PO_4/Al_2O_3$ | Glycerol; r.t. | 12 | 73 | 83 | [103] |
| **5g** | BS-2G-Ti | $H_2O$; 70 °C | 90 | 96 | 85 | [104] |
| **5g** | $BF_3$/MNPs-450 | EtOH; reflux | 10 | 90 | 87 | [105] |
| **5g** | Silica-bonded *N*-propyl-piperazine | EtOH; reflux | 15 | 88 | 86 | [106] |
| **5g** | $Fe_3O_4$@GO-*N*-(pyridin-4-amine) | $H_2O$; reflux | 20 | 98 | 91 | Present work |

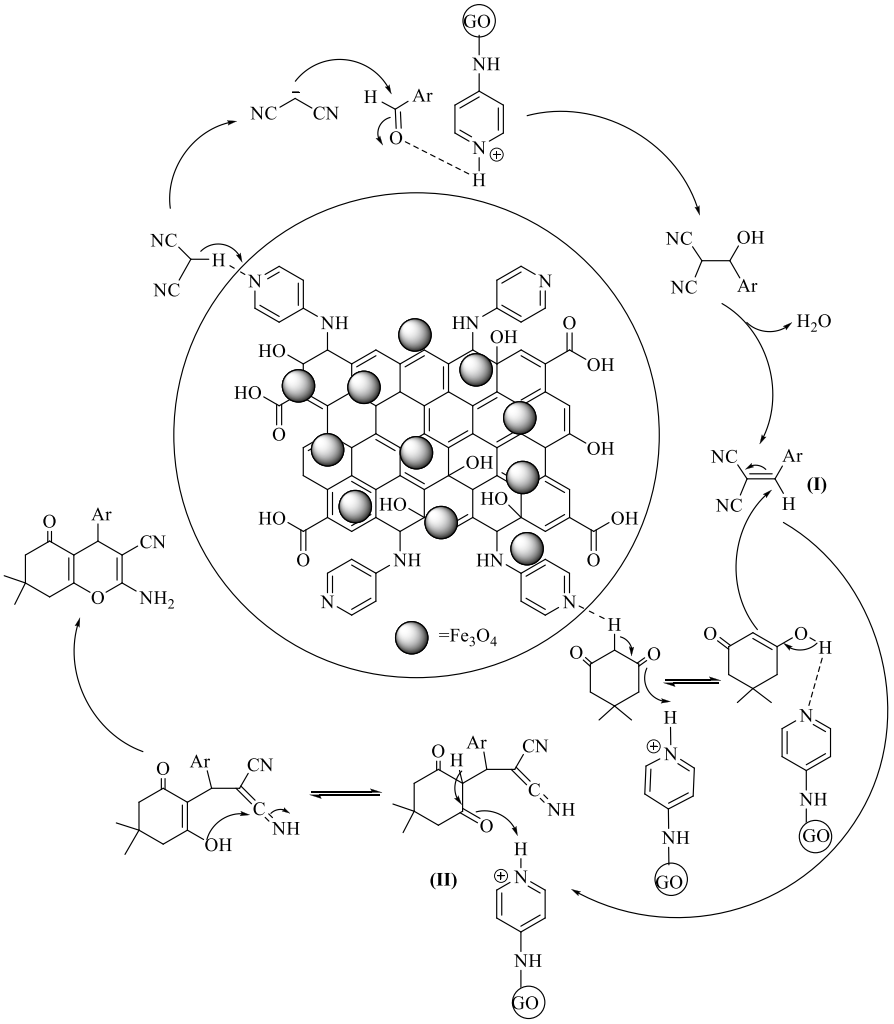


**Scheme 3** Possible mechanism for the synthesis of 2-amino-4-aryl-7,7-dimethyl-5-oxo-5,6,7,8-tetrahydro-4*H*-chromene-3-carbonitrile derivatives **4a**–**h** catalyzed by $Fe_3O_4$@GO-*N*-(pyridin-4-amine)

the reported method [107] demonstrates that our method is greener in comparison with other methods shown in Table 6.

## Catalytic reaction mechanism

Based on the mechanisms previously described by Rodrigo et al. [83] and other research groups [108–110], we propose a plausible mechanism to explain the $Fe_3O_4$@GO-*N*-(pyridin-4-amine)-catalyzed three-component synthesis of 2-amino-4-aryl-7,7-dimethyl-5-oxo-5,6,7,8-tetrahydro-4*H*-chromene-3-carbonitrile

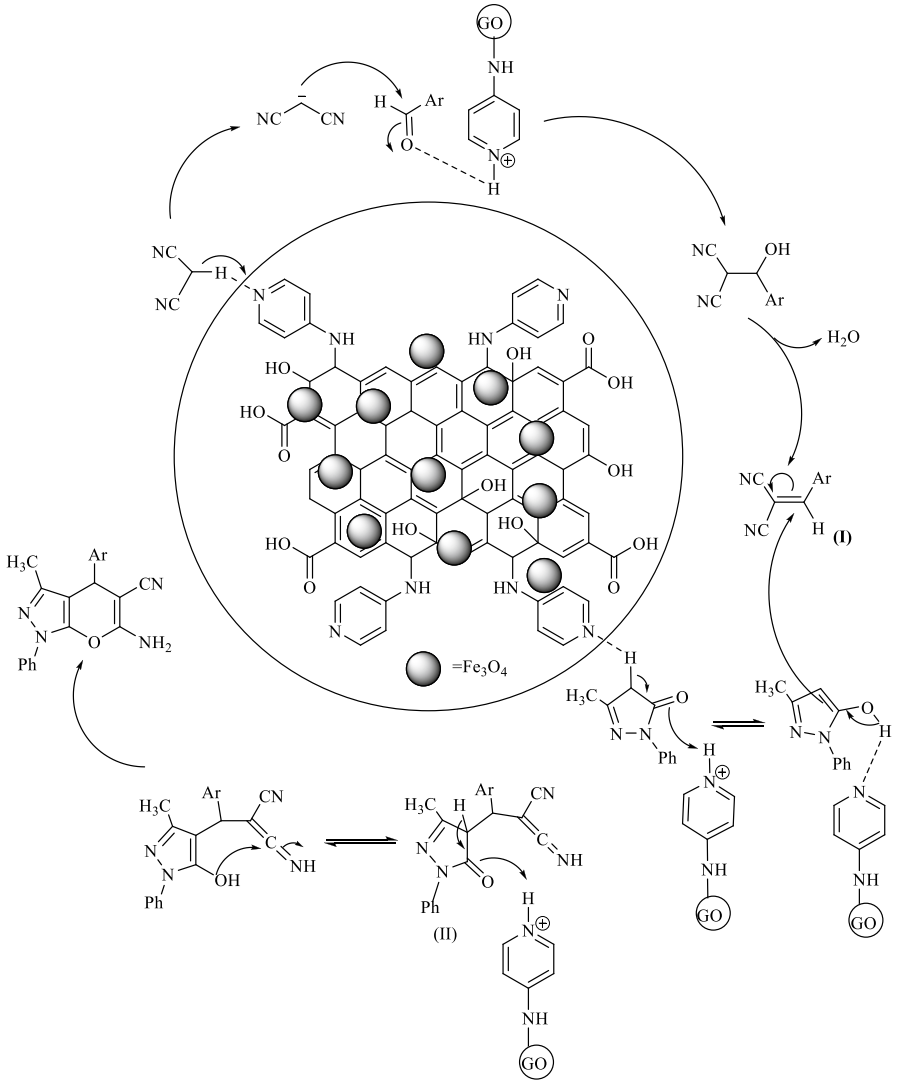


**Scheme 4** Possible mechanism for synthesis of 1,4-dihydropyrano[2,3-*c*]pyrazole derivatives **5a**–**h** catalyzed by $Fe_3O_4$@GO-*N*-(pyridin-4-amine)

derivatives **4a**–**h** in Scheme 3. The first step possibly involves deprotonation of malononitrile promoted by the graphene oxide-bonded aminopyridine moiety, which acts as Lewis base. Then, the resulting malononitrile anion reacts with the protonated aldehyde, leading to formation of α-cyanocinnamonitrile intermediate **I** after dehydration. Afterwards, aminopyridine-induced enolization of dimedone occurs to produce its enol form. This enol undergoes nucleophilic addition to intermediate **I** to

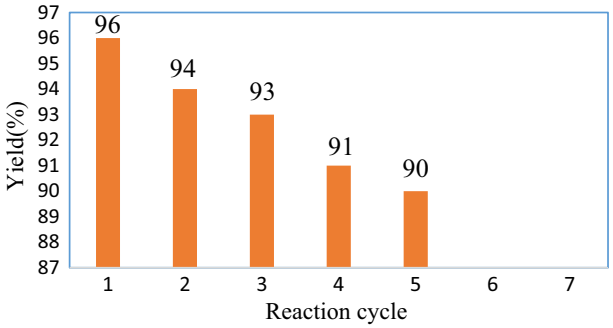


**Fig. 7** Recyclability of the catalyst $Fe_3O_4$@GO-*N*-(pyridin-4-amine) in model synthesis of 2-amino-4-(*p*-nitrophenyl)-7,7-dimethyl-5-oxo-5,6,7,8-tetrahydro-4*H*-chromene-3-carbonitrile (**4g**)

afford adduct **II**, which subsequently undergoes catalyzed intramolecular cyclization to yield the expected 4*H*-chromene derivatives **4a**–**h**.

A similar mechanism can be postulated for the $Fe_3O_4$@GO-*N*-(pyridin-4-amine)-catalyzed three-component synthesis of 1,4-dihydropyrano[2,3-*c*]pyrazole derivatives, as depicted in Scheme 4. In this mechanism, α-cyanocinnamonitrile intermediate **I** forms as described previously in Scheme 3, then reacts with the enolized form of methyl-1-phenyl-2-pyrazolin-5-one under catalytic effect of the catalyst. Finally, the resulting intermediate adduct **II** undergoes intramolecular cyclization in presence of the protonated catalyst to afford the expected products **5a**–**h**.

### Catalyst recyclability

The recyclability of the catalyst $Fe_3O_4$@GO-*N*-(pyridin-4-amine) was studied for the model reaction under the optimized conditions repeatedly. The change of catalytic activity in terms of yield against the number of cycles of the reaction is presented in Fig. 7. After reaction completion in each cycle, the catalyst was separated from the reaction mixture simply by using an external magnet. Then, the recovered catalyst was washed with hot ethanol and dried in oven at 70 °C. As shown in Fig. 7, the catalyst could be recycled and reused for at least five runs without considerable loss of activity. The slight decrease of catalytic activity could be due to normal loss of the catalyst during the workup stage.

## Conclusions

We report a novel preparation of 4-aminopyridine-grafted $Fe_3O_4$-magnetized graphene oxide [$Fe_3O_4$@GO-*N*-(pyridin-4-amine)]. The structure of the prepared $Fe_3O_4$@GO-*N*-(pyridin-4-amine) magnetic nanofilms was characterized by EDX, FT-IR, XRD, VSM, and SEM techniques. This new nanocatalyst exhibited high catalytic activity in three-component synthesis of 4*H*-chromenes and

dihydropyrano[2,3-*c*]pyrazole derivatives. The reactions proceeded smoothly in $H_2O$ as green solvent to afford the products in excellent yield. Green reaction conditions, high yield, simple magnetic separation of the catalyst from the reaction mixture, and easy recycling of the catalyst are considered as the main advantages of the present protocol.

**Acknowledgements** The authors wish to thank the Research Council of Bu-Ali Sina University for financial support to carry out this research. Also, Islamic Azad University, North Tehran Branch, is sincerely appreciated for technical support.

## References

1. K. Tanaka, F. Toda, Chem. Rev. **100**, 1025 (2000)
2. P.T. Anastas, J.C. Warner, *Green Chemistry, Theory and Practice* (Oxford University Press, Oxford, 1998)
3. P.T. Anastas, T. Williamson, *Green Chemistry, Frontiers in Benign Chemical Synthesis and Process* (Oxford University Press, Oxford, 1998)
4. G.A. Olah, A. Molnar, *Hydrocarbon Chemistry* (Wiley, New York, 1995)
5. A. Schatz, O. Reiser, W.J. Stark, Chem. Eur. J. **16**, 8950 (2010)
6. N. Yan, C.X. Xiao, Y.K. Coord, Chem. Rev. **254**, 1179 (2010)
7. C.O. Dalaigh, S.A. Corr, Y.G. Ko, S.J. Connon, Angew. Chem. Int. Ed. **46**, 4329 (2007)
8. F. Shi, M.K. Tse, M.M. Pohl, A. Bruckner, S. Zhang, M. Beller, Angew. Chem. Int. Ed. **46**, 8866 (2007)
9. D.H. Zhang, G.D. Li, J.X. Li, J.S. Chen, Chem. Commun. **29**, 3414 (2008)
10. M.R. Hoffman, S.T. Martin, W.D. Choi, W. Bahnemann, Chem. Rev. **95**, 69 (1995)
11. A. Saxena, A. Kumar, S. Mozumdar, J. Mol. Catal. A: Chem. **269**, 35 (2007)
12. A.T. Bell, Science **299**, 1688 (2003)
13. S. Shylesh, J. Schweizer, S. Demeshko, V. Schunemann, S. Ernst, W.R. Thiela, Adv. Synth. Catal. **351**, 1789 (2009)
14. V. Polshettiwar, R.S. Varma, Green Chem. **12**, 743 (2010)
15. D. Guin, B. Baruwati, S.V. Manorama, Org. Lett. **9**, 1419 (2007)
16. C.W. Lim, I.S. Lee, Nano Today. **5**, 412 (2010)
17. S. Shylesh, V. Schunemann, W.R. Thiel, Angew. Chem. **49**, 3428 (2010)
18. Y.H. Zhu, L.P. Stubbs, F. Ho, R.Z. Liu, C.P. Ship, J.A. Maguire, N.S. Hosmane, ChemCatChem **2**, 365 (2010)
19. V. Polshettiwar, R. Luque, A. Fihri, H.B. Zhu, M. Bouhrara, J.M. Bassett, Chem. Rev. **111**, 3036 (2011)
20. T.Q. Zeng, W.W. Chen, C.M. Cirtiu, A. Moores, G.H. Song, C.J. Li, Green Chem. **12**, 570 (2010)
21. L.M. Rossi, N.J.S. Costa, F.P. Silva, R.V. Goncalves, Nanotech. Rev. **2**, 597 (2013)
22. Y. Zhang, C.G. Xia, Appl. Catal. A **366**, 141 (2009)
23. S. Laurent, D. Forge, M. Port, A. Roch, C. Robic, L.V. Elst, R.N. Muller, Chem. Rev. **108**, 2064 (2008)
24. L. Ma'mani, M. Sheykhan, A. Heydari, M. Faraji, Y. Yamini, Appl. Catal. A **377**, 64 (2010)
25. B. Karimi, E. Farhangi, Chem. Eur. J. **17**, 6056 (2011)
26. G.B. Dharma, M.P. Kaushik, A.K. Halve, Tetrahedron Lett. **53**, 2741 (2012)
27. J.M. Khurana, K. Vij, Tetrahedron Lett. **52**, 3666 (2011)
28. B. Karami, K. Eskandari, S. Khodabakhshi, Arkivoc **ix**, 76 (2012)
29. A. Rashidi, Z. Tavakoli, Y. Tarak, S. Khodabakhshi, M.K. Abbasabadi, J. Chin. Chem. Soc. **63**, 399 (2016)
30. D.R. Dreyer, S. Park, C.W. Bielawski, R.S. Ruoff, Chem. Soc. Rev. **39**, 228 (2010)
31. D.R. Dreyer, H.P. Jia, C.W. Bielawski, Angew. Chem. Int. Ed. **49**, 6813 (2010)
32. A. Rashidi, M.K. Abbasabadi, S. Khodabakhshi, J. Nat. Gas Sci. Eng. **36**, 13 (2016)

33. K.S. Novoselov, A.K. Geim, S.V. Morozov, D. Jiang, M.I. Katsnelson, I.V. Grigorieva, S.V. Dubonos, A.A. Firsov, Nature **438**, 197 (2005)
34. K.S. Novoselov, Z. Jiang, Y. Zhang, S.V. Morozov, H.L. Stormer, U. Zeitler, J.C. Maan, G.S. Boebinger, P. Kim, A.K. Geim, Science **315**, 1379 (2007)
35. S. Stankovich, D.A. Dikin, G.H.B. Dommett, K.M. Kohlhaas, E.J. Zimney, E.A. Stach, R.D. Piner, S.T. Nguyen, R.S. Ruoff, Nature **442**, 282 (2006)
36. M.K. Abbasabadi, A. Rashidi, J. Safaei-Ghomi, S. Khodabakhshi, R. Rahighi, J. Sulfur Chem. **36**, 660 (2015)
37. D.W. Wang, F. Li, J.P. Zhao, W.C. Ren, Z.G. Chen, J. Tan, Z.S. Wu, I. Gentle, G.Q. Lu, H.M. Cheng, ACS Nano **3**, 1745 (2009)
38. I.V. Lightcap, T.H. Kosel, P.V. Kamat, Nano Lett. **10**, 577 (2010)
39. F. Hu, M. Patel, F. Luo, C. Flach, R. Mendelsohn, E. Garfunkel, H. He, M. Szostak, J. Am. Chem. Soc. **137**, 14473 (2015)
40. S. Khodabakhshi, F. Marahel, A. Rashidi, M.K. Abbasabadi, J. Chin. Chem. Soc. **62**, 389 (2015)
41. B. Majumdar, D. Sarma, T. Bhattacharya, T.K. Sarma, A.C.S. Sustain. Chem. Eng. **5**, 9286 (2017)
42. H. Hea, J. Klinowskia, M. Forsterb, A. Lerfb, Chem. Phys. Lett. **287**, 53 (1998)
43. L. Alvey, S. Prado, B. Saint-Joanis, S. Michel, M. Koch, S.T. Cole, F. Tillequin, Y.L. Janin, Eur. J. Med. Chem. **44**, 2497 (2009)
44. T. Narender, S.Gupta Shweta, Bioorg. Med. Chem. Lett. **14**, 3913 (2004)
45. H. Gourdeau, L. Leblond, B. Hamelin, C. Desputeau, K. Dong, I. Kianicka, D. Custeau, C. Boudreau, L. Geerts, S.X. Cai, J. Drewe, D. Labrecque, S. Kasibhatla, B. Tseng, Mol. Cancer Ther. **3**, 1375 (2004)
46. V.K. Tandon, M. Vaish, S. Jain, D.S. Bhakuni, R.C. Srimal, Indian J. Pharm. Sci. **53**, 22 (1991)
47. M. Rueping, E. Sugiono, E. Merino, Chem. Eur. J. **14**, 6329 (2008)
48. M.T. Flavin, J.D. Rizzo, A. Khilevich, A. Kucherenko, A.K. Sheinkman, V. Vilaychack, L. Lin, W. Chen, E.M. Greenwood, T. Pengsuparp, J.M. Pezzuto, S.H. Hughes, T.M. Flavin, M. Cibulski, W.A. Boulanger, R.L. Shone, Z.Q. Xu, J. Med. Chem. **39**, 1303 (1996)
49. M. Longobardi, A. Bargagna, E. Mariani, P. Schenone, S. Vitagliano, L. Stella, A. Di Sarno, E. Marmo, Farmaco **45**, 399 (1990)
50. J.M. Doshi, D. Tian, C. Xing, J. Med. Chem. **49**, 7731 (2006)
51. M.N. Erichsen, T.H.V. Huynh, B. Abrahamsen, J.F. Bastlund, C. Bundgaard, O. Monrad, A. Bekker-Jensen, C.W. Nielsen, K. Frydenvang, A.A. Jensen, L. Bunch, J. Med. Chem. **53**, 7180 (2010)
52. S.J. Mohr, M.A. Chirigos, F.S. Fuhrman, J.W. Pryor, Cancer Res. **35**, 3750 (1975)
53. L. Bonsignore, G. Loy, D. Secci, A. Calignano, Eur. J. Med. Chem. **28**, 517 (1993)
54. D.O. Moon, K.C. Kim, C.Y. Jin, M.H. Han, C. Park, K.J. Lee, Y.M. Park, Y.H. Choi, G.Y. Kim, Int. Immunopharmacol. **7**, 222 (2007)
55. L.L. Andreani, E. Lapi, Bull. Chim. Farm. **99**, 583 (1960)
56. Y. Peng, G. Song, Catal. Commun. **8**, 111 (2007)
57. B.N. Seshu, N. Pasha, R.K.T. Venkateswara, P.P.S.N. Lingaiah, Tetrahedron Lett. **49**, 2730 (2008)
58. T.S. Jin, L.B. Liu, Y. Zhao, T.S. Li, Synth. Commun. **35**, 1859 (2005)
59. S. Banerjee, A. Horn, H.G. Khatri, Tetrahedron Lett. **52**, 1878 (2011)
60. L.M. Fotouhi, M. Heravi, A. Fatehi, K. Bakhtiari, Tetrahedron Lett. **48**, 5379 (2007)
61. F. Khorami, H.R. Shaterian, Chin. J. Catal. **35**, 242 (2014)
62. N.M.A. bdEi-Rahman, A.A. Ei-Kateb, M.F. Mady, Synth. Commun. **37**, 3961 (2007)
63. M. Khoobi, L. Ma'mani, F. Rezazadeh, Z. Zareie, A. Foroumadi, A. Ramazani, A. Shafiee, J. Mol. Catal. A: Chem. **359**, 74 (2012)
64. J.L. Wang, D. Liu, Z.J. Zhang, S. Shan, X. Han, S.M. Srinivasula, C.M. Croce, E.S. Alnemri, Z. Huang, Proc. Natl. Acad. Sci. U. S. A. **97**, 7124 (2000)
65. M.E.A. Zaki, H.A. Soliman, O.A. Hiekal, Z.A.E. Rashad, Naturforsch. C **61**, 1 (2006)
66. C.B. Sangani, D.C. Mungra, M.P. Patel, R.G. Patel, Chin. Chem. Lett. **23**, 57 (2012)
67. A.K. Elziaty, O.E.A. Mostafa, E.A. El-Bordany, M. Nabil, H.M.F. Madkour, Int. J. Sci. Eng. Res. **5**, 727 (2014)
68. S.C. Kuo, L.J. Huang, H. Nakamura, J. Med. Chem. **27**, 539 (1984)
69. D. Azarifar, Y. Abbasi, Synth. Commun. **46**, 745 (2016)
70. M.S. Shingare, D.V. Mane, Chin. Chem. Lett. **21**, 1175 (2010)
71. G. Vasuki, K. Kumaravel, Tetrahedron Lett. **49**, 5636 (2008)
72. S. Gogoi, C.G. Zhao, Tetrahedron Lett. **50**, 2252 (2009)
73. H. Sheibani, M. Babaie, Synth. Commun. **40**, 257 (2010)

74. T.S. Jin, R.Q. Zhao, T.S. Li, Arkivoc **xi**, 176 (2006)
75. D. Azarifar, M. Tadayoni, M. Ghaemi, Appl. Organomet. Chem. **32**, e4293 (2018)
76. D. Azarifar, R. Nejat-Yami, M. AlKobaisi, J. Iran. Chem. Soc. **10**, 439 (2013)
77. D. Azarifar, S.M. Khatami, R. Nejat-Yami, J. Chem. Sci. **126**, 95 (2014)
78. D. Azarifar, R. Nejat-Yami, F. Sameri, Z. Akrami, Lett. Org. Chem. **9**, 435 (2012)
79. D. Azarifar, M. Ghaemi, M. Golbaghi, R. Karamian, M. Asadbegy, RSC Adv. **6**, 92028 (2016)
80. S. Khodabakhshi, M. Khaleghi Abbasabadi, S. Heydarianc, S. Gharehzadeh Shirazi, F. Marahel, Lett. Org. Chem. **12**, 465 (2015)
81. W.S.J. Hummers, R.E. Offeman, J. Am. Chem. Soc. **80**, 1339 (1958)
82. M.K. Abbasabadi, A. Rashidi, S. Khodabakhshi, J. Nat. Gas Sci. Eng. **28**, 87 (2016)
83. E. Rodrigo, B.G. Alcubilla, R. Sainz, J.L.G. Fierro, R. Ferritto, M. BeleńCid, Chem. Commun. **50**, 6270 (2014)
84. M.Z. Kassaee, E. Motamedi, M. Majdi, Chem. Eng. J. **172**, 540 (2011)
85. G. Chen, S. Zhai, Y. Zhai, K. Zhang, Q. Yue, L. Wang, J. Zhao, H. Wang, J. Liu, J. Jia, Biosens. Bioelectron. **26**, 3136 (2011)
86. L.Z. Bai, D.L. Zhao, Y. Xu, J.M. Zhang, Y.L. Gao, L.Y. Zhao, J.T. Tang, Mater. Lett. **68**, 399 (2012)
87. S. Khodabakhshi, B. Karami, New J. Chem. **38**, 3586 (2014)
88. C. Hou, Q. Zhang, M. Zhu, Y. Li, H. Wang, Carbon **49**, 47 (2011)
89. D. Azarifar, Y. Abbasi, O. Badalkhani, J. Adv. Chem. **10**, 3197 (2014)
90. D. Fang, H.B. Zhang, Z.L. Liu, J. Hetrocycl. Chem. **47**, 63 (2010)
91. S. Khaksar, A. Rouhollahpour, S.M. Talesh, J. Fluor. Chem. **141**, 11 (2012)
92. S. Balalaie, M. Bararjanian, M. Sheikh-Ahmadi, S. Hekmat, P. Salehi, Synth. Commun. **37**, 1097 (2007)
93. S. Sarrafi, E. Mehrasbi, A. Vahid, M. Tajbakhsh, Chin. J. Catal. **33**, 1486 (2012)
94. T.S. Jin, A.Q. Wang, Z.L. Cheng, J.S. Zhang, T.S. Li, Synth. Commun. **35**, 137 (2005)
95. S.B. Guo, S.X. Wang, J.T. Li, Synth. Commun. **37**, 2111 (2007)
96. L.G. Sharanina, V.K. Promonenkov, V.P. Marshtupa, A.V. Pashchenko, V.V. Puzanova, A.Y. Sharanin, N.A. Klyuev, L.F. Gusev, A.P. Gnatusina, Chem. Heterocycl. Compd. **18**, 607 (1982)
97. A. Saha, S. Payra, S. Banerjee, Green Chem. **17**, 2859 (2015)
98. M. Farahi, B. Karami, I. Sedighimehr, H. Mohamadi Tanuraghaj, Chin. Chem. Lett. **25**, 1580 (2014)
99. M. Kangani, N. Hazeri, M. Taher Maghsoodlou, J. Chin. Chem. Soc. **63**, 896 (2016)
100. S.S. Pourpanah, S.M. Habibi-Khorassani, M. Shahraki, Chin. J. Catal. **36**, 757 (2015)
101. A.A. Mohammadi, M.R. Asghariganjeh, A. Hadadzahmatkesh, Arab. J. Chem. **10**, S2213 (2017)
102. J. Yang, S. Liu, H. Hu, S. Ren, A. Ying, Chin. J. Chem. Eng. **23**, 1416 (2015)
103. A. Abdel Hamid, M. Abd-Elmonem, A.M. Hayallah, F.A. Abo Elsoud, K.U. Sadek, Chem. Sel. **2**, 10689 (2017)
104. P.S. Sinija, K. Sreekumar, RSC Adv. **5**, 101776 (2015)
105. M. Abdollahi-Alibeik, A. Moaddeli, K. Masoomi, RSC Adv. **5**, 74932 (2015)
106. K. Niknam, N. Borazjani, R. Rashidian, A. Jamali, Chin. J. Catal. **34**, 2245 (2013)
107. K.V. Aken, L. Strekowski, L. Patiny, Beilstein J. Org. Chem. **2**, 3 (2006)
108. J. Huang, S. Ding, W. Xiao, Y. Peng, S. Deng, N. Zhang, Catal. Lett. **145**, 1000 (2015)
109. B. Xue, J. Zhu, N. Liu, Y. Li, Catal. Commun. **64**, 105 (2015)
110. H.M.A. Hassan, R.F.M. Elshaarawy, S. Kumar Dey, I. Simon, C. Janiak, Catal. Lett. **147**, 1998 (2017)